

HYDROGEN BALMER CONTINUUM IN SOLAR FLARES DETECTED BY THE
INTERFACE REGION IMAGING SPECTROGRAPH (IRIS)

P. HEINZEL

Astronomical Institute, Academy of Sciences of the Czech Republic
Fričova 298, 25165 Ondřejov, Czech Republic

L. KLEINT

University of Applied Sciences and Arts Northwestern Switzerland
Bahnhofstrasse 6, 5210 Windisch, Switzerland

ABSTRACT

We present a novel observation of the white-light flare (WLF) continuum, which was significantly enhanced during the X1 flare on March 29, 2014 (SOL2014-03-29T17:48). Data from the Interface Region Imaging Spectrograph (IRIS) in its NUV channel show that at the peak of the continuum enhancement, the contrast at the quasi-continuum window above 2813 Å reached 100 - 200 % and can be even larger closer to the Mg II lines. This is fully consistent with the hydrogen recombination Balmer continuum emission, which follows an impulsive thermal and non-thermal ionization caused by the precipitation of electron beams through the chromosphere. However, a less probable photospheric continuum enhancement cannot be excluded. The light curves of the Balmer continuum have an impulsive character with a gradual fading, similar to those detected recently in the optical region on Hinode/SOT. This observation represents a first Balmer-continuum detection from space far beyond the Balmer limit (3646 Å), eliminating seeing effects known to complicate the WLF detection. Moreover, we use a spectral window so far unexplored for flare studies, which provides the potential to study the Balmer continuum, as well as many metallic lines appearing in emission during flares. Combined with future ground-based observations of the continuum near the Balmer limit, we will be able to disentangle between various scenarios of the WLF origin. IRIS observations also provide a critical quantitative measure of the energy radiated in the Balmer continuum, which constrains various models of the energy transport and deposition during flares.

Subject headings: Sun: flares — techniques: spectroscopic

1. INTRODUCTION

Radiation emitted during a solar flare from the lower solar atmosphere (chromosphere and photosphere) represents a significant, if not dominant, portion of the total energy deposited in those layers by various mechanisms. Considering the standard collisional thick-target model (CTTM, Brown 1971), the electron beam transports the energy from the coronal reconnection site down to the lower atmosphere, where its energy is dissipated. The heated atmosphere produces strongly enhanced radiation in many spectral lines and various continua, but the emission also comes from direct non-thermal collisional excitations and ionizations of the plasma by the beam. The most spectacular visible-continuum emission is known as the white light flare (WLF), first detected by Carrington (1859). Two mechanisms are currently considered to be responsible for this optical emission (see, e.g., Ding 2007): (i) photospheric continuum enhancement as a signature of the temperature increase below the temperature minimum region (mainly the H⁻ continuum), and (ii) hydrogen recombination continua (Paschen, Balmer) produced in the chromosphere. The radiation in the latter continua emitted upwards can be directly detected, while the downward component is supposed to heat the photosphere, the so-called 'back-warming' (Machado et al. 1989). In EUV, the hydrogen emits a strong Lyman continuum below 912 Å and this was recently well detected by the SDO/EVE spec-

trometer (Milligan et al. 2012, 2014). A new attempt to estimate the energy contained in the optical continua was recently made using Hinode/SOT (Watanabe et al. 2013; Kerr & Fletcher 2014; Milligan et al. 2014). The spectral coverage is rather poor, but the data allow to estimate the total power by fitting the continuum with the black-body curve. However, such a black-body fit leads to a low enhancement in the Balmer continuum, contrary to numerical simulations of the hydrogen recombination continua, which predict much higher emission. Therefore, observations of the Balmer continuum during flares are highly desirable in order to set-up constraints on various mechanisms producing the WLFs.

Only few detections of the Balmer-continuum brightening during flares are described in the literature. All have been made from the ground and only close to the Balmer limit at 3646 Å. In some cases, the Balmer jump was detected, in others a smooth transition from the so-called 'blue continuum' (Donati-Falchi et al. 1985) to the Balmer continuum was observed (see summary by Neidig 1989; Kerr & Fletcher 2014). Quite recently, this was also detected by Kotrč et al. (2014) who measured the flux from the whole flare area. On the other hand, Svestka (1976) claims in his book that no Balmer continuum was detected in many flare spectra collected at the Ondřejov observatory. The detectability limit may be related to the photographic technique used, but others detected non-negligible enhancements (see e.g.,

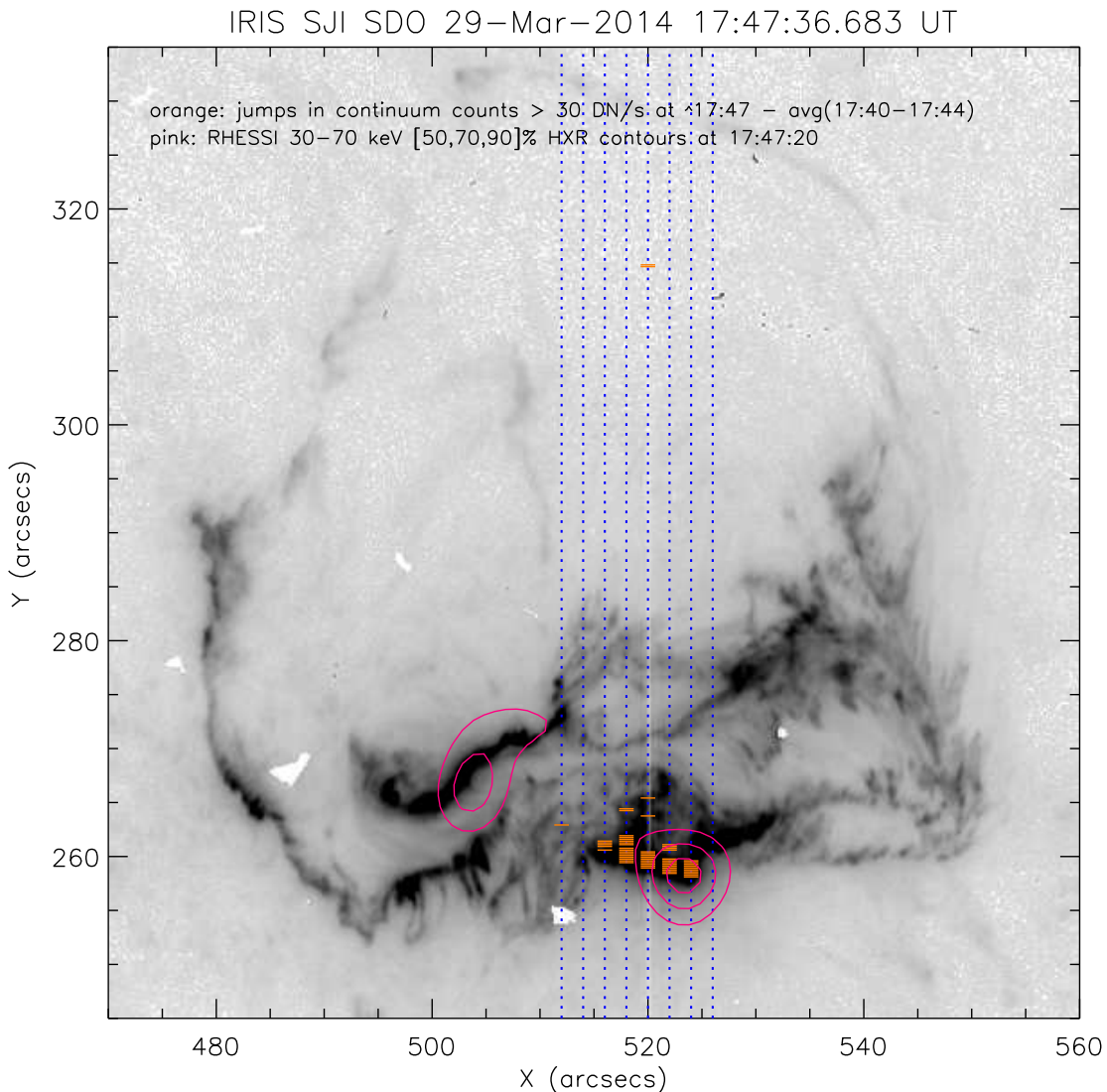


FIG. 1.— IRIS 1400 SJI with intensity reversed showing the flare ribbons in black. The intersections of the horizontal orange lines with the vertical IRIS slit positions (dotted blue) mark positions where the continuum increased significantly. Pink RHESSI 30–70 keV HXR contours are drawn for reference.

Zirin & Neidig 1981; Hiei 1982).

In this Letter we present a novel observation of the Balmer continuum, obtained from space and far beyond the Balmer limit. We therefore eliminate the seeing effects known to complicate WLF observations and simultaneously consider an unexplored spectral window. This was achieved using recent Interface Region Imaging Spectrograph (IRIS, De Pontieu et al. 2014) observations of a large X-class flare, and namely in the near-UV (NUV) channel suitable for the detection of the Balmer continuum. In this wavelength range, the expected WLF contrast is much higher compared to the visible part of the spectrum. Moreover, the IRIS slit is continuously scanning the flare area and thus we get an uninterrupted time evolution of the Balmer-continuum enhancement which we compare with RHESSI and GOES lightcurves.

2. IRIS OBSERVATIONS

The well-observed X1 flare on March 29, 2014 (SOL2014-03-29T17:48) occurred in NOAA AR 12017, with GOES X-ray flux enhancements starting around

17:35 UT and peaking at 17:48 UT. For a complete timeline of the event, see Kleint et al. (2014). IRIS was carrying out a coordinated observing program with the Dunn Solar Telescope and Hinode from 14:09 – 17:54 UT and captured the whole impulsive phase and part of the decay phase of the flare. The center of the flare was approximately located at coordinates (265" N, 515" W), which corresponds to (10.3° N, 32.9° W) and $\mu = \cos \theta = 0.83$.

The IRIS observation consisted of an 8-step raster in steps of 2". At each raster step, a far-UV spectrum (FUV), a near-UV spectrum (NUV), and a slitjaw image (SJI) was taken. The total field-of-view was 14" × 174" for the spectra and ~174 × 174" for each SJI image (see Fig. 1). The nominal exposure time of each image was 8 seconds, which, including overhead, yielded a cadence of 75 seconds per raster. During the flare, the NUV and SJI had automatic exposure control enabled, reducing their exposure times to minimize saturation of the images. The dispersion of the FUV and NUV spectra is 25.46 mÅ/px for this observation and the plate scale

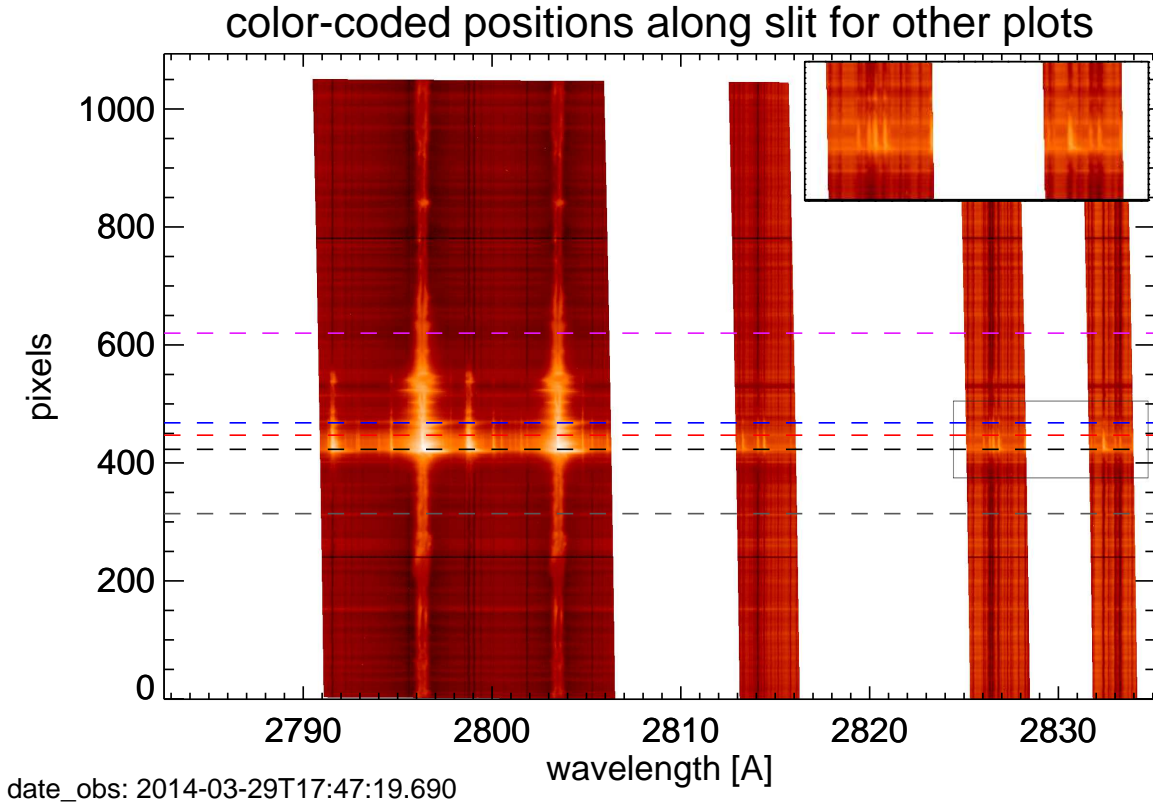


FIG. 2.— IRIS NUV spectrum showing the intensity enhancement throughout the whole spectrum, including the continuum, which was zoomed in on the top right. Reference positions for the following plots are indicated by horizontal lines.

is $0.166''/\text{px}$.

Here, we focus on the NUV spectra, which contain the two strong lines Mg II h and k and their extended wings with many blend lines. The NUV spectra may record wavelengths from 2783 – 2835 Å, but usually the detector is only read out partially to save time and down-link volume. For these observations, the “Flare linelist” was used, which saves four spectral ranges: $\sim 2791\text{--}2806$ Å, $\sim 2813\text{--}2816$ Å, $\sim 2825\text{--}2828$ Å, and $\sim 2831\text{--}2834$ Å, shown in Fig. 2 where white indicates parts of the detector that were not read out or saved. We used the calibrated Level 2 data, which include corrections for dark current, flatfield, geometry, but do not include an absolute radiometric calibration.

3. ANALYSIS OF THE IRIS FLARE SPECTRA

We analyzed the IRIS data for flare-related brightness increases in the continuum, defined as far wing of the Mg II line where no spectral lines are visible. This is usually called a ‘quasi-continuum’ and is well visible in a broader spectrum taken by HRTS-9 where the quasi-continuum peaks between the Mg II h and strong Mg I line (Morrill & Korendyke 2008). Figure 1 shows a (negative) SJI 1400 image, with the flare ribbons appearing in black. The white particles are dust on the camera. The eight vertical dotted lines mark the IRIS slit positions of the raster. The intersections of small orange horizontal lines with the slits mark locations where the continuum counts increased by at least 30 DN/s at $\sim 17:47$ UT compared to the average counts from $\sim 17:40\text{--}17:44$ UT. The exact times are different for each slit position be-

cause of the duration of the raster, e.g. for slit position 1 we looked at counts at 17:46:51 UT - avg(17:40:36 – 17:44:21 UT), while for position 8 it was 17:47:56 UT - avg(17:41:42 – 17:45:27 UT). The continuum enhancements clearly coincide with the flare ribbon. The pink contours show the RHESSI 30–70 keV HXR emission at [50, 70, 90]%, for context. While the location of HXR and continuum brightening agrees in general, a more detailed analysis that includes the motion of the HXR footpoints and the exact timing of each raster step will be carried out in the future to explore a possible relationship of the continuum brightness and the HXR emission.

Figure 2 shows the NUV spectrum at 17:47:19 UT with the two bright Mg II k and h lines and three spectral regions further in the h -wing to the red. An enhancement of brightness is clearly visible around $y=420$ px, not only in the spectral lines, but also in the continuum. The inset on the top right shows a magnified part of the spectrum denoted by the box. The horizontal color-coded lines refer to positions along the slit, which are used for the following analysis.

Figure 3 shows the NUV spectrum at the selected locations from Fig. 2. At the brightest positions along the slit (black line) the continuum counts are seen to increase by a factor of 2 - 3 compared to the quiet Sun (pink dotted line). The other spectra were chosen to show other bright flare regions (red dotted and blue lines), and a bright feature outside of the flare (grey line). The inset of the figure shows a magnification of the continuum regions. While many spectral lines go into emission during the flare (black, red, and blue spectra), the black and red

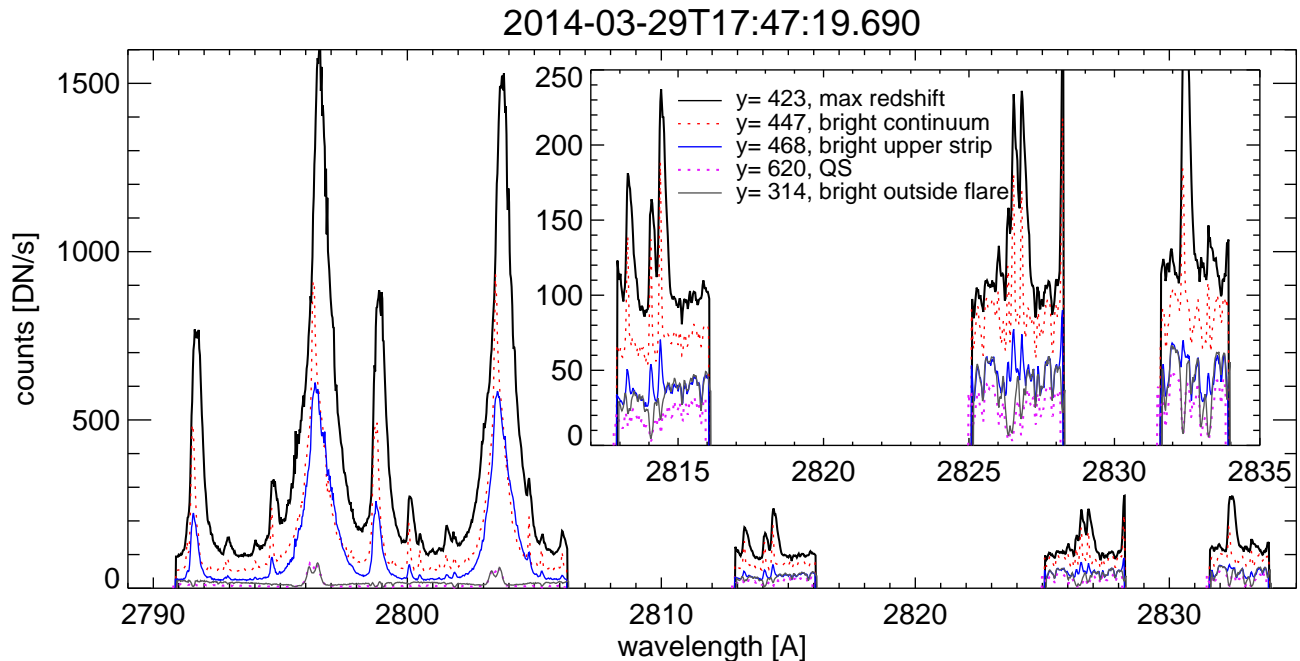


FIG. 3.— Example spectra during the flare at the five different positions along the slit indicated in Fig. 2. The continuum values are higher in the black and red spectra, which are from the flare footpoint. Note that the QS quasi-continuum increases with increasing wavelength which is due to the photospheric wing of the Mg II h line.

spectra also show an increased continuum, compared to the reference spectra from the quiet Sun (pink), and the bright feature (grey). Comparing the blue and the grey spectra, it seems that the only difference are the lines in emission, while the continuum is similar. In other words, the continuum between lines is not affected by the line emission itself.

Obviously, for a conclusive proof whether this continuum variation is due to the flare, it is necessary to investigate the temporal behavior, which is shown in Fig. 4. The lightcurves in counts/second (DN/s) are plotted for each of the five positions along the slit, which are again indicated in the magnified spectrum on the bottom right. The counts were averaged over a small region of the continuum at about 2825.7 – 2825.8 Å (denoted by white vertical lines in the spectrum) and plotted for each time when the slit was at the same position (raster step 4). The lightcurves in the top row ($y=423$ and $y=447$) clearly show a strong increase in continuum counts by about a factor of two. The lightcurve from $y=468$ may show a very small increase too and the reference spectra (QS at $y=620$ and bright feature at $y=314$) do not show any flare-related changes. For reference, the plots also include the GOES X-ray curve (orange) and the RHESSI corrected count rates of 25-50 keV (purple), both in arbitrary units. However, these were derived by averaging over the whole active region only to show that the continuum variations are indeed flare-related while a more detailed analysis will be carried out in the future to analyze RHESSI lightcurves at each pixel.

We can also investigate if the continuum increase shows any spectral characteristics by subtracting a QS spectrum at each timestep. From Fig. 4 we know that the QS did not vary significantly during the flare. For Fig. 5, we therefore subtracted the QS from a spectrum in the

flare ribbon ($y=447$) to obtain the absolute change in counts per second over the whole spectral range. Before the flare, the difference was about 20 DN/s, and it increased during the flare to over 80 DN/s. All panels of Fig. 5 show a uniform increase of the different continuum regions, indicating that there is no detectable spectral dependence of the continuum brightness (within this limited spectral range). The spectral lines obviously vary more. A constancy of the difference spectra indicates no brightening of the far h -line wing itself during the flare.

4. HYDROGEN RECOMBINATION CONTINUUM

Assuming the recombination model, we can compare quantitatively the theoretical predictions with our results. For this we first convert the observed continuum enhancement to *cgs units* of $\text{erg sec}^{-1} \text{cm}^{-2} \text{sr}^{-1} \text{Å}^{-1}$. In Fig. 4 we show the lightcurves measured as the spectrum average in a narrow ‘quasi-continuum’ window between 2825.7 and 2825.8 Å. The quiet-Sun level ($y=620$) is somewhat varying with time having an average level around 50 DN/s (note that all estimates here are made for the actual position of the flare on the disk which is $\mu=0.83$). Using recent results of HRTS-9 quiet-Sun observations, we derived the corresponding disk intensity at $\mu = 0.83$ and at our ‘quasi-continuum’ window as 3.7×10^5 cgs units - see Fig. 11 and 14a in Morrill & Korendyke (2008). In their Fig. 13c, our narrow window is also indicated as a quasi-continuum. The lightcurve at flare position $y=447$ peaks at the level 115 and subtracting the pre-flare level 60 we get the pure continuum enhancement 55 DN/s which corresponds to 4.1×10^5 cgs units.

The NLTE modeling of the Balmer recombination continuum formed during flares was performed by various authors, see a review by Ding (2007). Here

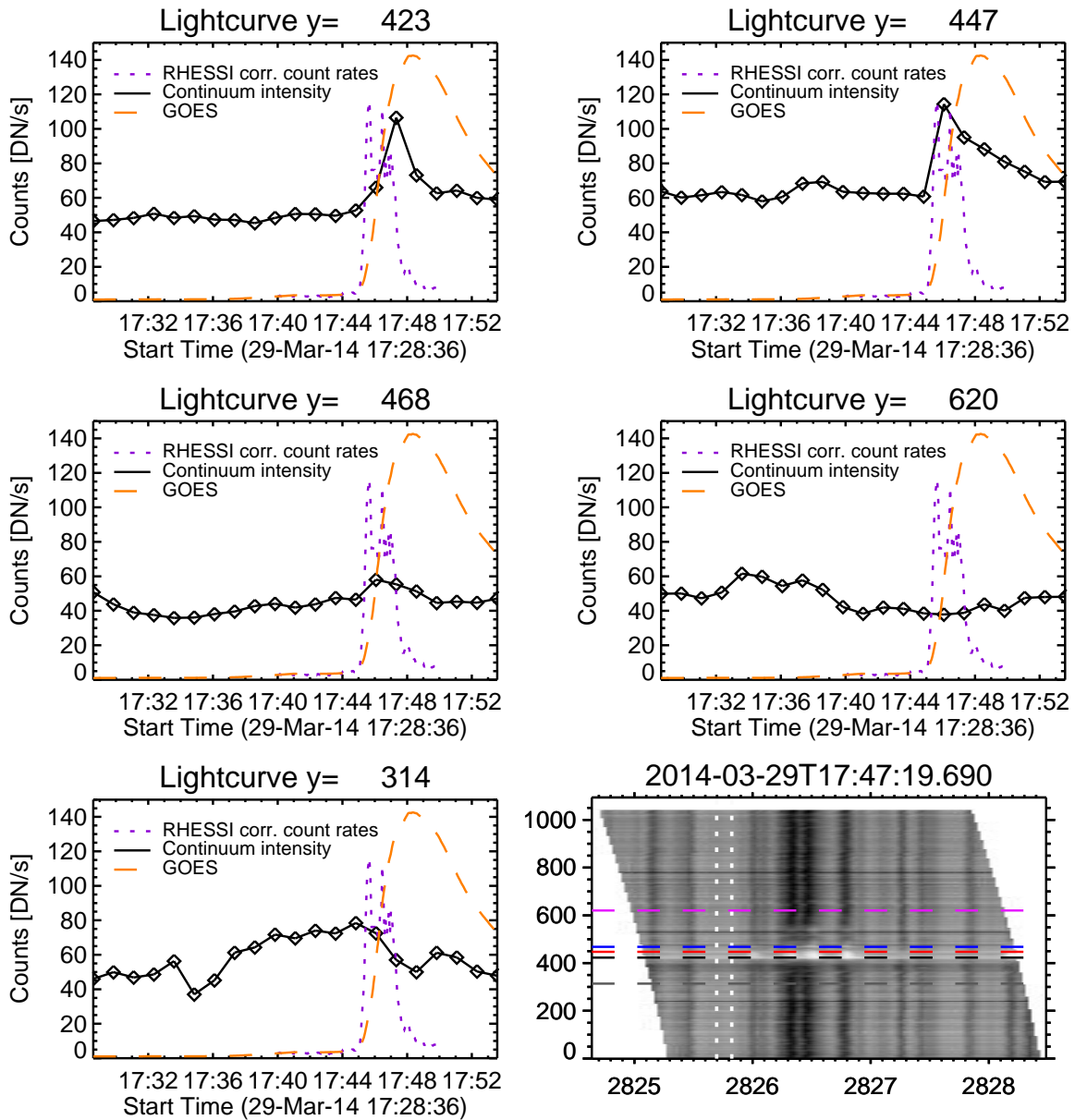


FIG. 4.— Lightcurves of the continuum intensity (defined as the average between the two white dotted vertical lines on the bottom right) at five positions along the slit (pixel coordinates given in title of each plot). A comparison with GOES and RHESSI lightcurves is also shown.

we use the results based on static flare models of Ricchiazzi & Canfield (1983), who constructed a grid of models in energy balance with the electron-beam (CCTM) and conductive energy deposit in the lower atmospheric layers. As an example, we considered their model E4 with the electron-beam flux F_{20} equal to 10^{11} erg sec $^{-1}$ cm $^{-2}$ and the spectral index $\delta = 5$. A preliminary calculation of RHESSI energy deposition rates yields the same order of magnitude for this flare (S. Krucker, private communication). Using the MALI (Multilevel Accelerated Lambda Iteration) NLTE technique and including the non-thermal collisional rates for hydrogen, we computed the intensity of the recombination Balmer continuum for this specific model (see also Heinzel & Kašparová 2014). At our continuum window, this intensity is equal to 3.2×10^5 cgs units and the emit-

ting chromospheric layer has the optical thickness around 0.1, i.e. is optically thin as expected. We thus see that this theoretical value is very much consistent with the observed enhancement 4.1×10^5 cgs units. Note that by increasing the pressure in coronal loops above the model chromosphere, one can achieve more than a factor of two enhancement of the Balmer continuum within the emitting layer. Our results are also in good agreement with previous semi-empirical NLTE modeling of Avrett et al. (1986) who obtained a similar Balmer continuum enhancement for their model F2, but for very strong flares (model F3) the enhancement is a factor of three larger. In case of optically-thin emitting layers, the theoretical flare contrast in the Balmer continuum dramatically increases with decreasing μ and this will help the continuum detection when the flare is observed close to the

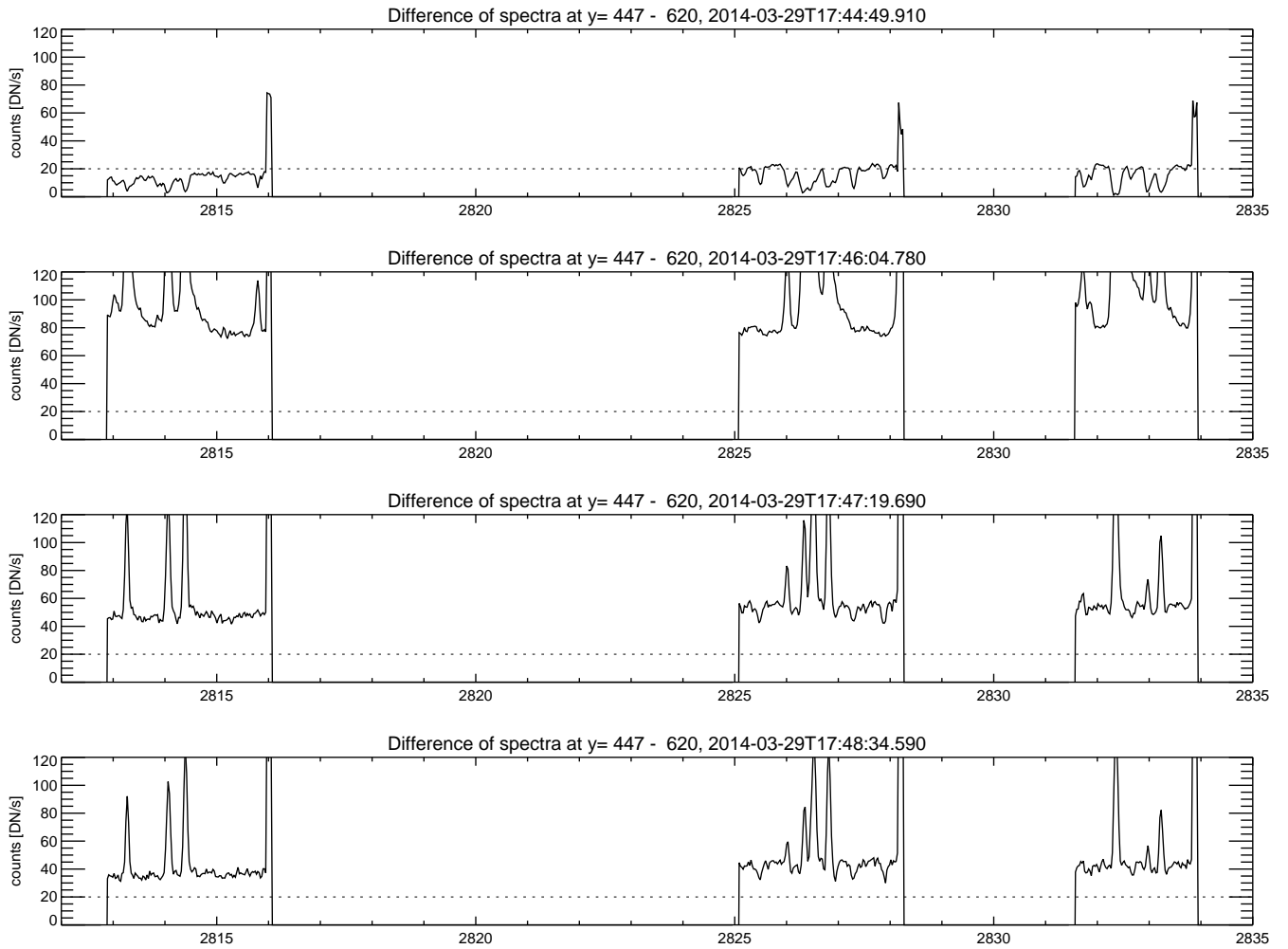


FIG. 5.— Difference of a spectrum in the flare ribbon ($y=447$ px) and the quiet Sun ($y=620$ px) at each timestep given in the title. A uniform increase of the continuum (between lines) in the whole spectral region is clearly visible. The dashed line is drawn for reference to indicate the approximate pre-flare value.

limb.

We have also tested the absolute radiometric calibration of IRIS within the NUV window using a conversion curve between DN/s and our cgs units, the factor is 2.23×10^4 which gives the QS level 1.1×10^6 cgs units, three times larger than the HRTS-9 value. This then implies a stronger enhancement of the flare continuum which could be explained with other models. The IRIS calibration was performed before launch and is estimated to be accurate within a factor of two, while HRTS-9 was cross-calibrated via SUSIM/UARS, which in turn was calibrated via SOLSTICE/UARS, so both methods may have similar error bars.

5. DISCUSSION AND FUTURE PROSPECTS

Visual inspection of the IRIS spectrum in Fig. 2 taken just after at the flare HXR maximum immediately suggests that there is a considerable continuum enhancement at locations of strong Mg II line emission. This is evident at the three narrower spectral windows relatively far from the the position of Mg II lines. However, there are also some other locations outside the flare region which exhibit brighter continua, actually there are

many such bright strips in this example spectrum. This is not surprising because the photospheric continuum in this UV spectral range varies even for quiet-Sun spectra. However, we have shown that the enhancements at flare positions significantly exceed the other structural variations and, most critically, they vary in accordance with the flare evolution. Moreover, at flare positions 423 and namely at 447 we have identified unambiguous impulsive increase of the continuum emission, consistent with the HXR and GOES variations. We consider this an evidence of the continuum brightening at flare locations.

This impulsive increase and a gradual decrease look qualitatively similar to those recently found by Kerr & Fletcher (2014) (see their Fig. 5 and 6) for the 15 February 2011 X2.2 flare observed in the visible continuum by Hinode/SOT. As a potential source of the WLF emission, they consider the Paschen continuum which is emitted by an optically-thin slab producing hydrogen recombination radiation. The same process was considered for interpreting our observations in the Balmer continuum. Further radiation-hydrodynamical (RHD) simulations are required to predict the light curves of Balmer and Paschen continua, consistently with time evolution of

the electron-beam energy deposition. The latter is usually derived from RHESSI spectra and drives the RHD simulations (Varady et al. 2010; Milligan et al. 2014).

There might be a question whether the continuum enhancement is not an artifact of a flare brightening in the wings of the Mg II lines. From previous observations (Lemaire et al. 1984) and from our NLTE simulations it seems to be unlikely that very far photospheric wings of these lines (i.e. up to 30 Å from the Mg II *h* line center) go into emission. Such an emission should also gradually decrease with the increasing distance from the line center. We thus tested the excess emission in Fig. 5 and found that at time of maximum continuum enhancement, it is constant over the passband of our three windows. This suggests that we see the Balmer continuum emission added on top of the quiet photospheric spectrum in the far wing of the MgII *h* line. Regarding the possible influence of the numerous metallic lines which go into emission during the flare (Fig. 3), we postpone this question to a future study where we plan to compute the complete synthetic flare spectrum in the whole NUV window. Currently, we can only estimate a negligible contribution of the metallic line wings to the continuum brightness. First, we saw in Section 3 that pixels 314 and 468 have the same enhanced continuum while the flare pixel shows several metallic lines in emission. The other argument is based on synthetic spectra of the semi-empirical flare model F3 (Avrett et al. 1986), where some metallic lines are in strong emission without any effect on the surrounding continuum level.

While we focused on the NUV spectra, IRIS also records FUV spectra from ~ 1331 – 1358 Å and ~ 1380 – 1407 Å. These data, which are not shown here, also show a significant brightness enhancement in the continuum, with similar timings as the NUV. But in the FUV wavelength range, there likely is a strong contribution from the optically thick continua from silicon and carbon (Vernazza et al. 1981), while the Balmer continuum

contribution is expected to be small in the FUV during flares. So it would be very hard to disentangle these contributions, which is why the NUV window is much better suited for the Balmer continuum detection and therefore used in this exploratory letter.

In this study we have detected a significant brightness enhancement in the IRIS NUV continuum during an X-class flare. We exclude a possible influence of metallic line emission and show quantitatively that the observed enhancement is quite consistent with the height-integrated emissivity of the hydrogen recombination Balmer continuum. However, we cannot a priori exclude a possible, but according to models less probable enhancement of the photospheric continuum (quasi-continuum in our case, represented by the far wings of the Mg II lines). Therefore, it is highly desirable to detect the Balmer continuum at least at two distant wavelengths, one being the IRIS NUV window and the other near the Balmer limit currently detectable by some ground-based instruments. The IRIS NUV window is very promising for future flare research, providing a unique flare diagnostics of the Balmer continuum, as well as of many metallic lines, including Mg II *h* and *k*.

This work was supported by the FP-7 collaborative project No. 606862 'F-CHROMA' (PH) and by ASI ASCR project RVO:67985815 (PH). LK was supported by a Marie-Curie Fellowship and by the NASA grant NNX13AI63G. We would like to thank Marina Battaglia for providing the RHESSI corrected count rates and the HXR contours. We also thank Sam Krucker and the anonymous referee for valuable comments. IRIS is a NASA small explorer mission developed and operated by LMSAL with mission operations executed at NASA Ames Research center and major contributions to down-link communications funded by the Norwegian Space Center (NSC, Norway) through an ESA PRODEX contract.

REFERENCES

- Avrett, E. H., Machado, M. E., & Kurucz, R. L. 1986, in *The lower atmosphere of solar flares*, p. 216 - 281, ed. D. F. Neidig, 216–281
- Brown, J. C. 1971, *Sol. Phys.*, 18, 489
- Carrington, R. C. 1859, *MNRAS*, 20, 13
- De Pontieu, B., Title, A. M., Lemen, J. R., et al. 2014, *Sol. Phys.*, 289, 2733
- Ding, M. D. 2007, in *Astronomical Society of the Pacific Conference Series*, Vol. 368, *The Physics of Chromospheric Plasmas*, ed. P. Heinzel, I. Dorotović, & R. J. Rutten, 417
- Donati-Falchi, A., Falciani, R., & Smaldone, L. A. 1985, *A&A*, 152, 165
- Heinzel, P., & Kašparová. 2014, in preparation
- Hiei, E. 1982, *Sol. Phys.*, 80, 113
- Kerr, G. S., & Fletcher, L. 2014, *ApJ*, 783, 98
- Kleint, L., Battaglia, M., Reardon, K., et al. 2014, *ApJ*, submitted
- Kotrč et al. 2014, in preparation
- Lemaire, P., Choucq-Bruston, M., & Vial, J.-C. 1984, *Sol. Phys.*, 90, 63
- Machado, M. E., Emslie, A. G., & Avrett, E. H. 1989, *Sol. Phys.*, 124, 303
- Milligan, R. O., Chamberlin, P. C., Hudson, H. S., et al. 2012, *ApJ*, 748, L14
- Milligan, R. O., Kerr, G. S., Dennis, B. R., et al. 2014, *ArXiv e-prints*
- Morrill, J. S., & Korendyke, C. M. 2008, *ApJ*, 687, 646
- Neidig, D. F. 1989, *Sol. Phys.*, 121, 261
- Ricchiuzzi, P. J., & Canfield, R. C. 1983, *ApJ*, 272, 739
- Svestka, Z. 1976, *Geophysics and Astrophysics Monographs*, 8
- Varady, M., Kasparova, J., Moravec, Z., Heinzel, P., & Karlicky, M. 2010, *IEEE Transactions on Plasma Science*, 38, 2249
- Vernazza, J. E., Avrett, E. H., & Loeser, R. 1981, *ApJS*, 45, 635
- Watanabe, K., Shimizu, T., Masuda, S., Ichimoto, K., & Ohno, M. 2013, *ApJ*, 776, 123
- Zirin, H., & Neidig, D. F. 1981, *ApJ*, 248, L45